JPE 19-5-16

https://doi.org/10.6113/JPE.2019.19.5.1224
ISSN(Print): 1598-2092 / ISSN(Online): 2093-4718

Seamless Transition Strategy for Wide Speed-Range Sensorless IPMSM Drives with a Virtual Q-axis Inductance

Hanlin Shen*, Jinbang Xu*, Baiqiang Yu†, Qipeng Tang**, Bao Chen*, Chun Lou***, and Yu Qiao***

†,*School of Artificial Intelligence and Automation, Huazhong University of Science and Technology, Wuhan, China
**College of Electrical Engineering, Zhejiang University, Hangzhou, China
***State Key Laboratory of Coal Combustion, Huazhong University of Science and Technology, Wuhan, China

Abstract

Hybrid rotor position estimation methods that integrate a fundamental model and high frequency (HF) signal injection are widely used for the wide speed-range sensorless control of interior permanent-magnet synchronous machines (IPMSMs). However, the direct transition of two different schemes may lead to system fluctuations or system instability since two estimated rotor positions based on two different schemes are always unequal due to the effects of parameter variations, system delays and inverter nonlinearities. In order to avoid these problems, a seamless transition strategy to define and construct a virtual q-axis inductance is proposed in this paper. With the proposed seamless transition strategy, an estimated rotor position based on a fundamental model is forced to track that based on HF signal injection before the transition by adjusting the constructed virtual q-axis inductance. Meanwhile, considering that the virtual q-axis inductance changes with rotor position estimation errors, a new observer with a two-phase phase-locked loop (TP-PLL) is developed to accurately obtain the virtual q-axis inductance online. Furthermore, IPMSM sensorless control with maximum torque per ampere (MTPA) operations can be tracked automatically by selecting the proper virtual q-axis inductance. Finally, experimental results obtained from an IPMSM demonstrate the feasibility of the proposed seamless transition strategy.

Key words: IPMSM, Seamless transition, Sensorless, Virtual q-axis inductance

I. INTRODUCTION

The high-performance control of IPMSMs is commonly employed in power drive systems due to its high power density and efficiency. With the necessary information in the field-oriented control, the rotor position is often obtained from a mechanical sensor mounted on the rotor shaft. However, the presence of such sensors has disadvantages such as adding to the total cost and machine size. The sensors also limit its application in environments with high temperature, high humidity and high vibration. Moreover, the resolver or encoder signal wiring also reduces the reliability of commissioned drive systems. Therefore, various methods have been developed to achieve the sensorless control of IPMSMs [1]-[26].

Depending on the operation speed region, sensorless control methods can be roughly divided into two categories: high-frequency (HF) carrier signal injection methods based on saliency tracking and methods based on the fundamental model of an IPMSM. For the HF carrier signal injection methods, the rotor position is obtained from a position-dependent signal obtained by injecting HF excitation signals into a machine to interact with the saliency. These methods show good performance in the low-speed region, including zero speed. In addition, based on the different types of injected

Manuscript received Nov. 30, 2018; accepted Apr. 19, 2019
Recommended for publication by Associate Editor Gaolin Wang.
†Corresponding Author: ybqhust@foxmail.com
Tel: +86-027-8754-1547, Fax: +86-027-8754-1547, Huazhong Univ. of Science and Tech.
*School of Artificial Intelligence and Automation, Huazhong University of Science and Technology, China
**College of Electrical Engineering, Zhejiang University, China
***State Key Laboratory of Coal Combustion, Huazhong University of Science and Technology, China

carrier signals, these methods can be further classified into four different types: rotating HF signal injection in the stationary reference frame [1]-[4], pulsating signal injection in the stationary reference frame [5], pulsating signal injection in the estimated synchronous reference frame [6]-[8] and square wave signal injection [9], [10]. However, in these HF signal injection methods, a certain amount of dc-bus voltage is used to excite the saliency signal for acquisition of rotor position information, which not only increases the losses, torque ripple and transient disturbances but also limits its performance when the speed increases. Thus, HF signal injection methods are usually used for startup. The methods based on a fundamental model mainly include the state observer [11], disturbance observer [12], [13], Kalman filter [14]-[16], model reference adaptive method [17], sliding mode observer [18], [19], etc. These methods have the advantages of simplicity and straightforwardness. In addition, they can work reasonably well at medium and high speeds. However, they fail in the low-speed region and usually suffer from starting problems since the reduction and eventual disappearance of the back electromotive force (EMF) is too small to give reliable information on rotor position at low or zero speeds.

Therefore, in order to achieve wide speed-range sensorless control of IPMSMs, a combination of HF signal injection methods and methods based on a fundamental model has attracted a lot of attention. In [20], a hybrid structure integrating a flux observer and signal-injection techniques was presented to implement wide speed-range sensorless control of a surface mounted PMSM including zero-speed operation. A smooth transition can be achieved by incorporating an injection estimate as a part of the flux observer. In [21], a novel stator flux observer with a variable structure was proposed to achieve motion-sensorless direct-torque control of IPMSMs in wide speed regions. This observer employs a combined voltage-current model with a PI compensator at low speed. In addition, it gradually switches to a PI compensated closed-loop voltage model as the speed increases. In [22], an innovative sensorless two-degree-of-freedom current control scheme for the entire speed range was proposed. The scheme consists of a model-based dynamic feedforward control to set the reference response and to model the reference tracking controllers providing disturbance rejection and position error signals. A linear active disturbance rejection controller combing high-frequency current injection with EMF estimation was presented to achieve high performance IPMSM sensorless control in the full-speed range [23]. In order to achieve smooth operation between a saliency-based drive and an EMF-based drive, a transition method based on a single-phase-locked loop (PLL) with a speed-dependent weighting function was developed in [24] to blend saliency and EMF signals for position estimation.

This paper aims to improve the transition of HF carrier signal injection methods and methods based on a fundamental model for stable and reliable sensorless drives in a wide speed range. At zero and low speed, the saliency-tracking position estimation method based on rotating HF voltage injection is used to implement the field-oriented control algorithm. When the speed rises to medium or high speeds, a seamless transition is developed to convert a saliency-based drive using rotating HF voltage injection to a drive based on a fundamental model. In [26], virtual q-axis inductance, which is obtained based on virtual high frequency signal injection, is utilized to settle the observed flux angle so it can coincide with the MTPA angle. In this paper, virtual q-axis inductance is introduced to solve the transition problem between two estimation method. It is constructed to force the estimated rotor position based on a fundamental model to track that based on rotating HF voltage injection before the transition. Meanwhile, since the virtual q-axis inductance changes with rotor position estimation errors, a new observer with a TP-PLL is presented to accurately acquire the virtual q-axis inductance online. Furthermore, IPMSM sensorless control with MTPA operations can be tracked automatically by selecting a proper virtual q-axis inductance. Finally, the feasibility and effectiveness of the proposed seamless transition strategy are validated on an IPMSM.

This paper is arranged as follows. In section II, the conventional rotating HF carrier injection method and the position estimation method based on a fundamental model are described. A seamless transition strategy for the two schemes is presented in section III. In addition, the construction and acquisition of the virtual q-axis inductance are analyzed in detail. In order to improve the efficiency of the system, the sensorless control of PMSMs with MTPA trajectory are described in section IV. In section V, experimental results verify the effectiveness of the proposed seamless transition strategy. Finally, some conclusions are made in section VI.

II. Conventional Sensorless Control Methods for IPMSMs

A. Mathematical Model of an IPMSM

Regardless of the cross-coupling and multi-saliency of a machine, the basic model of an IPMSM can be described as Eqn. (1) in the d-q synchronous reference frame.

$$\begin{bmatrix} V_d \\ V_q \end{bmatrix} = \begin{bmatrix} R_s & -\omega_r L_q \\ \omega_r L_d & R_s \end{bmatrix} \begin{bmatrix} i_d \\ i_q \end{bmatrix} + \begin{bmatrix} L_d & 0 \\ 0 & L_q \end{bmatrix} \frac{d}{dt} \begin{bmatrix} i_d \\ i_q \end{bmatrix} + \begin{bmatrix} 0 \\ \omega_r \lambda_{pm} \end{bmatrix} \quad (1)$$

Where V_d, V_q, i_d, i_q, R_s, L_d, L_q, ω_r, λ_{pm} and d/dt are the d-axis voltage, q-axis voltage, d-axis current, q-axis current, stator resistance, d-axis inductance, q-axis inductance, rotor speed, flux linkage of the rotor magnet without stator current and derivative operator, respectively. By using a rotating inverse coordinate transformation, Eqn. (1) can be transformed to the stationary frame (α–β), which is expressed as Eqn. (2).

$$\begin{bmatrix} V_\alpha \\ V_\beta \end{bmatrix} = R_s \begin{bmatrix} i_\alpha \\ i_\beta \end{bmatrix} + \frac{d}{dt} \left\{ \begin{bmatrix} L_{\Delta+} - L_{\Delta-}\cos 2\theta_r & -L_{\Delta-}\sin 2\theta_r \\ -L_{\Delta-}\sin 2\theta_r & L_{\Delta+} + L_{\Delta-}\cos 2\theta_r \end{bmatrix} \cdot \begin{bmatrix} i_\alpha \\ i_\beta \end{bmatrix} + \lambda_{pm} \begin{bmatrix} \cos\theta_r \\ \sin\theta_r \end{bmatrix} \right\} \quad (2)$$

With $L_{\Delta+} = \frac{L_d + L_q}{2}$, $L_{\Delta-} = \frac{L_q - L_d}{2}$

Where V_α, V_β, i_α and i_β are the α-axis voltage, β-axis voltage, α-axis current and β-axis current, respectively. In addition, θ_r is the angle deviation between the actual d-axis and the α-axis, namely the rotor position of the motor.

B. Rotating HF Voltage Injection Method for Low-speed Control

Under the assumptions of a zero or low rotor speed and a high carrier frequency, so the back EMF and resistive voltage drop can be neglected, the basic model of an IPMSM can be simplified as Eqn. (3).

When a rotating high frequency carrier signal, described as Eqn. (4a), is injected into the machine, the HF response currents can be deduced as Eqn. (4b).

$$\begin{bmatrix} V_{\alpha h} \\ V_{\beta h} \end{bmatrix} = \begin{bmatrix} L_{\Delta+} - L_{\Delta-}\cos 2\theta_r & -L_{\Delta-}\sin 2\theta_r \\ -L_{\Delta-}\sin 2\theta_r & L_{\Delta+} + L_{\Delta-}\cos 2\theta_r \end{bmatrix} \frac{d}{dt} \begin{bmatrix} i_{\alpha h} \\ i_{\beta h} \end{bmatrix} \quad (3)$$

$$v_{\alpha\beta h} = V_c e^{j\omega_c t} \quad (4a)$$

$$i_{\alpha\beta h} = I_p e^{j\left(\omega_c t - \pi/2\right)} + I_n e^{j\left(-\omega_c t + 2\theta + \pi/2\right)} \quad (4b)$$

With:

$$I_n = \frac{V_c L_{\Delta-}}{\omega_c L_d L_q}, \qquad I_p = \frac{V_c L_{\Delta+}}{\omega_c L_d L_q}$$

Where ω_c and V_c are the frequency and amplitude of the injected rotating HF carrier signal, respectively. As can be seen from Eqn. (4b), the rotor position information is only contained in the second component. Thus, by using a coordinate transformation and a low-pass filter to extract the position-dependent component of Eqn. (4b), the rotor position information can be obtained as:

$$I_n^c = LPF\{i_{\alpha\beta h} \cdot e^{j\omega_c t}\} = I_n e^{j\left(2\theta + \pi/2\right)} \quad (5a)$$

$$2\theta_{rInj} = Arg\left(I_n^c\right) - \pi/2 \quad (5b)$$

Where *LPF* and *Arg(x)* represent a low-pass filter and the phase angle of vector x, respectively. A PLL is one of the practical implementations of *Arg(x)*. Finally, the estimated rotor position θ_{rInj} can be acquired accurately with a number of magnetic detection methods. It is noteworthy that the rotating high frequency carrier signal injection method is only applicable at zero and low speeds because there might be not enough dc-bus voltage, which can be used for voltage injection due to the high EMF voltage magnitude as the machine accelerates to high speeds.

C. Position Estimation Method based on a Fundamental Model for High-speed Control

When the machine runs at medium and high speeds, the back EMF is large enough to be used for the calculation of the rotor position. A simple model can be used to obtain the rotor position by calculating the flux that is induced by the rotor magnets into the stator winding. Firstly, the mathematical model Eqn. (2) can be rewritten as:

$$V_{\alpha\beta} = R_s i_{\alpha\beta} + L_q \frac{di_{\alpha\beta}}{dt} + \frac{d\lambda_{Ext}}{dt} \quad (6)$$

The extended flux λ_{Ext} can be computed as the integral of the back EMF of the machine and the compensation of the flux generated by the stator currents, which is given by Eqn. (7). Then, the rotor position can be calculated by Eqn. (8).

$$\lambda_{Ext} = \int \left(V_{\alpha\beta} - R_s i_{\alpha\beta}\right) dt - L_q i_{\alpha\beta} \quad (7)$$

$$\theta_{rEmf} = Arg\left(\lambda_{Ext}\right) \quad (8)$$

Generally, in the practical implementation of the extended flux λ_{Ext}, commanded voltages are used instead of actual measured values, and a low-pass filter is adopted to avoid drifting of the pure integrator in Eqn. (7). However, the adopted low-pass filter may bring phase and altitude deviations, which lead to estimation errors of the rotor position. In addition, it is worth noting that the use of a low-pass filter for the approximation of a pure integrator limits its effectiveness to fundamental frequencies that are well above the cutoff frequency of the filter. Therefore, a compensation strategy is used to solve these problems. Firstly, a low-pass filter with a variable low-gain $K\omega_r$ is used instead of the pure integrator in Eqn. (7). In this case, K is a constant. Its value range is generally from 0.3 to 1.0. The low-gain of the low-pass filter is adjusted proportionally to the rotating frequency. For the sake of analysis, using a Laplace transform to deal with Eqn. (7) yields:

$$\lambda_{Ext}(s) = \frac{M}{s + K\omega_r}\left(V_{\alpha\beta} - R_s i_{\alpha\beta}\right) - L_q i_{\alpha\beta} \quad (9)$$

With $M = (1 + K\omega_r/\boldsymbol{s})$.

The complex number M is calculated by $M/(s+K\omega_r)$ and it is equal to 1/s, which means the aim is to eliminate deviations coming from the LPF. On other hand, M is just a compensation term for the new variable LPF. When the machine runs in the steady state, the Laplace operator s is equivalent to $j\omega_r$. Substituting $s = j\omega_r$ into M, the complex number M is calculated as $(1-jK)$, which is constant. Thus, the effects of the adopted low-pass filter on the extended flux λ_{Ext} can be easily eliminated with the direct compensation of the constant M.

It should be noted that position estimation methods based a fundamental model only work reasonably well at medium and high speeds since the back EMF signal is too small to give reliable information about the rotor position at low speeds or

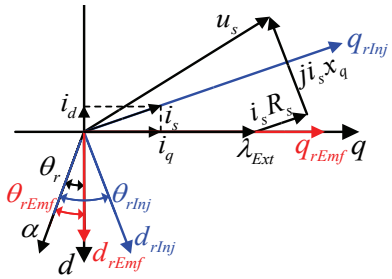

Fig. 1. Spatial relations of θ_r, θ_{rInj} and θ_{rEmf} in the low speed region.

zero speed. Thus, a combination of methods based on a fundamental model and high frequency carrier signal injection methods is commonly used to implement the sensorless control of IPMSMs from zero speed to high speeds. However, in practical applications, estimated rotor positions based on a high frequency carrier signal injection method θ_{rInj} are usually not equal to the actual rotor position θ_r due to some adverse impacts such as sampling delays of current sensors, transmission delays of hardware systems, parametric uncertainties and inverter nonlinearities. Considering that θ_{rInj} and i_d =0 are used to implement the field-oriented control of the IPMSM when the machine runs at low speeds, their spatial relationships between and among θ_r, θ_{rInj} and θ_{rEmf} can be roughly described in Fig. 1. Where u_s, i_s and x_q represent the stator voltage vector, current vector and q-axis inductive impedance.

It can be observed from Fig. 1 that there are some deviations between θ_{rInj} and θ_{rEmf}. If direct switching between θ_{rInj} and θ_{rEmf} is implemented when the machine runs from low speeds to high speeds, it can lead to system fluctuations, even system instability due to the equality of θ_{rInj} and θ_{rEmf}. Thus, the seamless transition of θ_{rInj} and θ_{rEmf} is especially important for smooth and stable sensorless control from low speeds to high speeds.

III. Seamless Transition Strategy

The inequality of θ_{rInj} and θ_{rEmf} is the main reason why direct transition between methods based on a fundamental model and high frequency carrier signal injection methods cannot be implemented. If θ_{rEmf} is made equal to θ_{rInj} before a transition, the seamless transition of two different schemes can be easily implemented without system fluctuations or system instability. Therefore, in order to realize smooth and stable wide speed-range sensorless control of IPMSMs, a seamless transition strategy to define and construct a virtual q-axis inductance is proposed in this section.

A. Virtual Q-axis Inductance

Estimated rotor positions based on a fundamental model θ_{rEmf} always have some deviations relative to actual rotor positions θ_r since the stator resistance R_s and inductance L_q change with the application environments. Thus, the spatial relationships of θ_r, θ_{rInj} and θ_{rEmf} can be roughly re-described in Fig. 2.

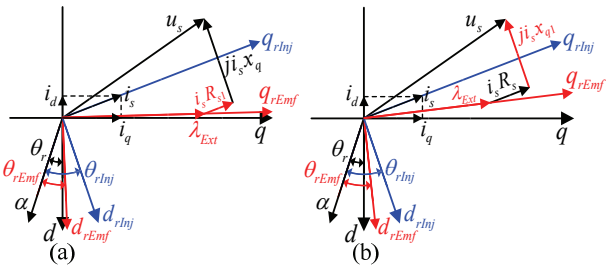

Fig. 2. Spatial relations of θ_r, θ_{rInj} and θ_{rEmf} in the low speed region. (a) Inaccurate stator resistance R_s. (b) Inaccurate stator inductance L_q.

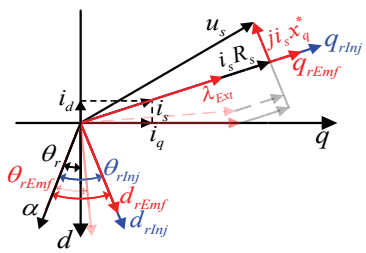

Fig. 3. Adjusting L_q to make θ_{rEmf} equal to θ_{rInj}.

As observed from Fig. 2, the estimated rotor position θ_{rEmf} is changes with an inaccurate stator resistance R_s and inductance L_q. In addition, according to the above analysis, the inequality of θ_{rInj} and θ_{rEmf} is the main reason leading to unstable switching of two estimation methods. If θ_{rEmf} is made equal to θ_{rInj} before the transition of two estimation methods by adjusting the stator resistance R_s or stator inductance L_q, the transition of θ_{rInj} and θ_{rEmf} can be easily implemented. However, it can be found from Fig. 2(a) that θ_{rEmf} cannot be equal to θ_{rInj} by only adjusting the stator resistance R_s. In addition, θ_{rEmf} can be equal to θ_{rInj} only by adjusting the stator inductance L_q, as shown in Fig. 3. However, in practical applications, L_q is the inherent characteristic of IPMSMs, which is not artificially changed. Therefore, in order to make θ_{remf} equal to θ_{rInj}, a virtual q-axis inductance $L_{q\_virtual}$ is defined and constructed.

Here $\varphi_{rInj\_err} = \theta_{rInj} - \theta_r$ and $\delta = (\theta_{rInj}+\pi/2-\theta_r)$. In addition, φ_{rInj_err} is the angle estimated error based on high frequency carrier signal injection methods.

When the actual L_q is used, the extended flux λ_{Ext} is obtained as Eqn. (10). On the other hand, the new extended flux λ_{Ext1} can be obtained as Eqn. (10) when $L_{q\_virtual}$ is used.

$$\begin{aligned} \lambda_{Ext} &= \int \left(V_{\alpha\beta} - R_s i_{\alpha\beta}\right) dt - L_q i_{\alpha\beta} \\ \left(\lambda_{pm} - 2L_{\Delta\_} i_d\right) \cdot e^{j\theta_r} &= \int \left(V_{\alpha\beta} - R_s i_{\alpha\beta}\right) dt - L_q I_s e^{j(\theta_r+\delta)} \\ \left(\lambda_{pm} - 2L_{\Delta\_} I_s \cos\delta\right) \cdot e^{j\theta_r} &= \int \left(V_{\alpha\beta} - R_s i_{\alpha\beta}\right) dt - L_q I_s e^{j(\theta_r+\delta)} \end{aligned} \tag{10}$$

$$\begin{aligned} \lambda_{Ext1} &= \int \left(V_{\alpha\beta} - R_s i_{\alpha\beta}\right) dt - L_{q\_virtual} i_{\alpha\beta} \\ \lambda_1 \cdot e^{j\theta_{rEmf}} &= \int \left(V_{\alpha\beta} - R_s i_{\alpha\beta}\right) dt - L_{q\_virtual} I_s e^{j(\theta_r+\delta)} \end{aligned} \tag{11}$$

Then it is possible to obtain λ_1 as Eqn. (12) and $\varphi_{rEmf\_err} = \theta_{rEmf} - \theta_r$ as Eqn. (13) by solving Eqn. (10) and Eqn. (11).

$$\lambda_1 = \sqrt{\left(L_q - L_{q\_virtual}\right)^2 \left(I_s \sin\delta\right)^2 + \left(\lambda_{pm} + \left(L_d - L_{q\_virtual}\right) I_s \cos\delta\right)^2} \quad (12)$$

$$\varphi_{rEmf\_err} = \tan^{-1} \frac{(L_q - L_{q\_virtual}) I_s \sin\delta}{\lambda_{pm} - (L_{q\_virtual} - L_d) I_s \cos\delta} \quad (13)$$

If $\theta_{rEmf} = \theta_{rInj}$ is substituted, that is $\varphi_{rEmf\_err} = \varphi_{rInj\_err} = \delta - \pi/2$, it is possible to obtain $L_{q\_virtual}$ as Eqn. (14) by solving Eqn. (13).

$$L_{q\_virtual} = L_q - \frac{\lambda_{pm} \sin\varphi_{rInj\_err}}{I_s} - 2L_{\Delta-}\left(\sin\varphi_{rInj\_err}\right)^2 \quad (14)$$

Considering that the amplitude of the stator current I_s can be sampled by a hall current sensor, the flux linkage of the rotor magnet λ_{pm}, L_q and L_d can be measured offline. If the angle estimated errors φ_{rInj_err} can be predicted or compensated, $L_{q\_virtual}$ can be calculated directly with reference to Eqn. (14). However, in practical applications, the prediction or compensation of φ_{rInj_err} is very inaccurate due to the influence of nonlinear factors, such as system delay, inverter nonlinearities, cross-coupling and multi-saliency of the machine. Thus, if offline calculation of $L_{q\_virtual}$ is adopted, the estimated rotor position θ_{rEmf} has large angle estimation errors. The angle deviations between θ_{rInj} and θ_{rEmf} can become larger, which results in system fluctuations or system instability, if the combination of two different estimation methods is used for wide speed-range sensorless operations. Thus, the real-time and accurate acquisition of $L_{q\_virtual}$ is a crucial factor to ensure the seamless transition of two rotor position estimation methods.

B. A New Observer with a TP-PLL

According to the above analysis, $L_{q\_virtual}$ is constructed to make θ_{rEmf} equal to θ_{rInj} before the machine switches to high speed from low speed. However, $L_{q\_virtual}$ cannot be calculated directly because of unknown rotor position estimation errors φ_{rInj_err}. In order to obtain a real-time and accurate $L_{q\_virtual}$, a new observer with a TP-PLL is presented in this section. A signal flowchart of the proposed observer is shown in Fig.4. The unit complex value of θ_{rInj} ($e^{j\theta rInj}$) is the given position signal, and the new extended flux λ_{Ext1} based on a fundamental model is the feedback position signal. Their vector cross-product is the input of the PLL and the output is the "virtual q-axis inductance" $L_{q\_virtual}$. Then, substitute $L_{q\_virtual}$ into Eqn. (11) to calculate a new extended flux λ_{Ext1}. Finally, θ_{rEmf} can be obtained by extracting the phase angle of λ_{Ext1}.

As can be observed from Fig. 4, the estimated expression of $L_{q\_virtual}$ can be expressed as:

$$L_{q\_virtual} = \frac{k_p s + k_i}{s^2}\left\{\lambda_1 \sin\left(\theta_{rEmf} - \theta_{rInj}\right)\right\} \quad (15)$$

Then, the actual calculation expression of $L_{q\_virtual}$ can be obtained as Eqn. (16) by rearranging Eqn. (13).

$$L_{q\_virtual} = L_q - \frac{\sin\varphi_{rEmf\_err}}{\cos\left(\varphi_{rInj\_err} - \varphi_{rEmf\_err}\right)}\left(2L_{\Delta-}\sin\varphi_{rInj\_err} + \frac{\lambda_{pm}}{I_s}\right) \quad (16)$$

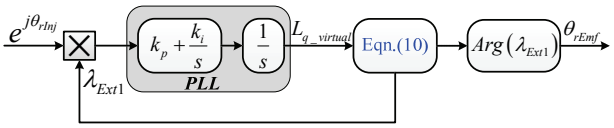

Fig. 4. New observer with a TP-PLL for accurate acquisition of $L_{q\_virtual}$.

In order to unify the variables of Eqn. (15) and Eqn. (16), Eqn. (15) can be re-expressed as Eqn. (17) since

$(\theta_{rEmf} - \theta_{rInj}) = (\theta_{rEmf} - \theta) - (\theta_{rInj} - \theta) = (\varphi_{rEmf\_err} - \varphi_{rInj\_err})$ is always true.

$$L_{q\_active} = \frac{k_p s + k_i}{s^2}\left\{\lambda_1 \sin\left(\varphi_{rEmf\_err} - \varphi_{rInj\_err}\right)\right\} \quad (17)$$

Then, when the proposed observer tends to be in the steady state, θ_{rEmf} is close to θ_{rInj} and the assumptions that $\cos(\varphi_{rEmf\_err} - \varphi_{rInj\_err}) \approx 1$ and $\sin(\varphi_{rEmf\_err} - \varphi_{rInj\_err}) \approx (\varphi_{rEmf\_err} - \varphi_{rInj\_err})$ are considered. Generally, $\sin(\varphi_{rEmf\_err})$ can be approximately equal to φ_{rEmf_err} and the high order components $\sin(\varphi_{rEmf\_err})$ and $\sin(\varphi_{rInj\_err})$ can be neglected since the two estimated rotor position errors φ_{rEmf_err} and φ_{rInj_err} are not very large. Then, combining Eqn. (16) with Eqn. (17) yields:

$$\frac{k_p s + k_i}{s^2}\lambda_1\left(\varphi_{rEmf\_err} - \varphi_{rInj\_err}\right) \approx L_q - \frac{\lambda_{pm}}{I_s}\varphi_{rEmf\_err} \quad (18)$$

Considering that the switching of θ_{rEmf} and θ_{rInj} is implemented in the low speed range, as long as the bandwidth of the proposed observer is much greater than the switching speed of the machine ω_{switch}, θ_r can be regarded as a constant during operation of the proposed observer. In addition, the closed-loop transfer function between θ_{rEmf} and θ_{rInj} can be equivalent to that of φ_{rEmf_err} and φ_{rInj_err}. Therefore, the dynamic and steady-state performances of the proposed observer, as shown in Fig. 4, can be described by the closed-loop transfer function between φ_{rEmf_err} and φ_{rInj_err}. Then, arranging Eqn. (18) yields:

$$\varphi_{rEmf\_err} = \frac{\left(k_p s + k_i\right)\lambda_1 I_s}{\left(k_p s + k_i\right)\lambda_1 I_s + \lambda_{pm} s^2}\varphi_{rInj\_err} + \frac{L_q I_s s^2}{\left(k_p s + k_i\right)\lambda_1 I_s + \lambda_{pm} s^2} \quad (19)$$

As can be observed from Eqn. (19), the first component is dominant in the low speed region, and the second component is dominant in the high speed region. Both them are related to φ_{rInj_err}, I_s, k_p, k_i, λ_{pm} and the motor running speed ω_r. Since the switching of θ_{rEmf} and θ_{rInj} is implemented in the low speed region, the second component of Eqn. (19) can be neglected before switching, and the closed-loop transfer function between φ_{rEmf_err} and φ_{rInj_err} can be expressed as:

$$\frac{\varphi_{rEmf\_err}}{\varphi_{rInj\_err}} = \frac{\left(k_p s + k_i\right)\lambda_1 I_s}{\left(k_p s + k_i\right)\lambda_1 I_s + \lambda_{pm} s^2} \quad (20)$$

In order to ensure that the proposed observer is stable, all of its eigenvalues should be on the left half of the complex plane. Thus, the following expression should be satisfied:

$$\frac{k_p \lambda_1 I_s}{\lambda_{pm}} > 0, \quad \frac{k_i \lambda_1 I_s}{\lambda_{pm}} > 0 \tag{21}$$

Because the magnitude of the transient current I_s and the magnitude of the new extended flux (λ_{Ext1}) λ_1 are always positive, the expression in Eqn. (21) can be guaranteed by selecting positive coefficients of k_p and k_i.

C. Parameters Design of the Proposed Observer

In the above section, the closed-loop transfer function between φ_{rEmf_err} and φ_{rInj_err} can be used to describe the dynamic and steady-state performances of the proposed observer based on the assumption that the bandwidth of the proposed observer is much greater than the switching speed of the machine ω_{switch}. If this assumption is invalid, the stability of the proposed observer cannot be described by Eqn. (20). Therefore, in order to make this assumption valid, the bandwidth of the proposed observer should be discussed.

According to the knowledge of classical control theory, the bandwidth frequency of the closed-loop transfer function in Eqn. (20) can be calculated as:

According to engineering experience, in order to make the above-mentioned assumption valid, the bandwidth frequency ω_b should be designed to be ten times larger than ω_{switch}. In other words, the following expression is obtained:

Eqn. (23) gives the basic requirement for the selections of k_p and k_i. Generally, a suitable switching speed ω_{switch} for the transition of θ_{rEmf} and θ_{rInj} is at least five percent of the rated speed ω_{rated}. As can be observed from Eqn. (22), the bandwidth frequency ω_b is directly proportional to the magnitude of the transient current I_s. If the machine runs at no-load or light load, the load current I_s is small, which leads to a minimum bandwidth frequency ω_b. Thus, in order to ensure that Eqn. (23) is valid under different load conditions, the selections of k_p and k_i can be designed based on the maximum possible estimated rotor position errors φ_{rInj_err} under the minimum load conditions.

D. Comparison with Existing Transition Strategies

There are two typical existing transition schemes: direct transition and weighting function based transition. Direct transition is fast and simple to implement. When the speed increases up to certain switching frequency $\omega_{\_switch}$, θ_{rInj} is directly switched to θ_{rEmf}. Deviation of the calculated angles in both methods results in a sudden change of the current or speed which can cause vibrations that are unacceptable for a lot of applications.

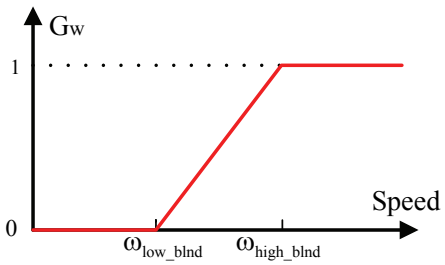

Fig. 5. Illustration of the speed dependent weighting function G_w.

The second method is to blend the angles obtained from the two methods into one angle in a transition region. A typical weighting function is used to blend angles just like Fig. 5. When the motor speed rise between ω_{low_blnd} and ω_{high_bld}, the rotor position is calculated as Eqn. (24). This measure can relief fluctuations caused by sudden changes of the angle/speed. However, the selection of low speed and high speed borders and weighting functions is difficult and mainly dependent on experience. The second deficiency is that the accuracy of the angle in the transition section depends on both of the methods. It further increases the difficulty to choose the proper transition region.

$$\hat{\theta}_r = \theta_{remf} G_w + \theta_{rinj}(1 - G_w) \tag{24}$$

The proposed method can always make the angle error of two sensorless algorithms become almost 0 before switching. This avoids the vibrations caused by sudden changes of the rotor position and speed. In addition, only one switching point can make the selection of the switching region unnecessary and transition section very smooth.

In Part V, results of the transition section of these 3 methods are compared to verify the analysis in Fig. 11~13.

IV. MTPA

Generally, as a strict performance index, the maximum efficiency control of IPMSMs is increasingly concerned with industrial applications due to the global energy shortage. Optimized control of IPMSMs can be achieved by proper selection of the current space vector as a function of the torque operating condition, often aiming at maximization of the ratio between the produced torque and the current amplitude, i.e., the maximum torque per ampere (MTPA). In principle, the MTPA control of PMSMs should be implemented over the entire speed range. However, in the actual applications, the rotor position estimation method based on high frequency carrier signal injection is usually

$$\omega_b^2 = \frac{\lambda_1 I_s}{2\lambda_{pm}^2}\left(2k_i\lambda_{pm} + k_p^2\lambda_1 I_s + \sqrt{8k_i^2\lambda_{pm}^2 + 4k_i k_p^2 \lambda_{pm}\lambda_1 I_s + k_p^4 \lambda_1^2 I_s^2}\right) \tag{22}$$

$$\frac{\lambda_1 I_s}{2\lambda_{pm}^2}\left(2k_i\lambda_{pm} + k_p^2\lambda_1 I_s + \sqrt{8k_i^2\lambda_{pm}^2 + 4k_i k_p^2 \lambda_{pm}\lambda_1 I_s + k_p^4 \lambda_1^2 I_s^2}\right) > 0.01\omega_{rswitch}^2 \tag{23}$$

used to start up the machine. After startup, the machine runs for a long time in the middle-high speed region, where the rotor position is estimated based on a fundamental model of PMSMs. Therefore, sensorless control of PMSMs with MTPA operations at middle-high speeds is analyzed in this section.

Firstly, when the machine operates in the steady state, the electromagnetic torque T_e can be calculated as:

$$T_e = \frac{3}{2} n_p \psi_{pm} i_q + \frac{3}{2} n_p \left(L_d - L_q\right) i_d i_q \tag{25}$$

Where n_p the number of pole pairs. The electromagnetic torque T_e consists of two parts: field torque from the permanent magnet and reluctance torque. The field torque, as expressed in the first term of Eqn. (25), is proportional to the q-axis current. The reluctance torque, as presented in the second term of Eqn. (25), is proportional to the multiplication of the d-axis current with the q-axis current. When the machine runs along the MTPA trajectory, the first-order differentiation of the torque with respect to the current vector angle δ should be zero, and is given as follows:

$$\frac{\partial T_e}{\partial \delta} = \frac{3}{2} n_p I_s \left[\lambda_{pm} \cos\delta + \left(L_d - L_q\right) I_s \cos 2\delta\right] = 0 \tag{26}$$

Then, the calculation expression of the current angle along the MTPA trajectory δ_{MTPA} can be derived as Eqn. (27) by solving Eqn. (26).

$$\delta_{MTPA} = \cos^{-1}\left(\frac{-\lambda_{pm} + \sqrt{\lambda_{pm}^2 + 8\left(L_d - L_q\right)^2 I_s^2}}{4\left(L_d - L_q\right) I_s}\right) \tag{27}$$

Therefore, the machine is always running along the MTPA trajectory as long as the current angle can meet the expression in (27). Considering that θ_{rEmf} and i_d =0 are used to implement the field-oriented control of the IPMSM when the machine runs at middle-high speeds, the current angle δ relative to the d-q synchronous reference frame is equal to (θ_{rEmf} + π/2 - θ_r). Then, substituting δ = (θ_{rEmf} + π/2 - θ_r) into Eqn. (27) and combining this with Eqn. (13) yields:

$$L_{q\_virtual} = L_q + \frac{C^2 - 4 - C\sqrt{C^2+8}}{4} L_{\Delta-} \tag{28}$$

With C =λ_{pm}/(2$I_s L_{\Delta-}$).

Because λ_{pm}, L_d, L_q and $L_{\Delta-}$ can be obtained from the manufacturer, and the magnitude of the stator transient current I_s can be sampled by current sensors, the value of $L_{q\_virtual}$ can be calculated offline by reference to Eqn. (28). Once $L_{q\_virtual}$ is obtained, the sensorless control of PMSMs with MTPA operations can be automatically tracked.

The proposed MTPA method show its advantages when combined with sensorless applications. In traditional sensorless applications with MTPA control, the rotor position and the MTPA trajectory angle have to be estimated. Then, the error of the estimated rotor position obviously interferes with the implementation of MTPA control. For the whole system, the error of these two parts is added and amplified.

TABLE I
CALCULATION OF VIRTUAL Q-AXIS INDUCTANCE

Computing stage	Transition section	MTPA control
Computing method	Output from TP-PLL, illustrated in Fig. 4	$L_{q\_virtual} = L_q + \frac{C^2 - 4 - C\sqrt{C^2+8}}{4} L_{\Delta-}$ C =λ_{pm}/(2$I_s L_{\Delta-}$)

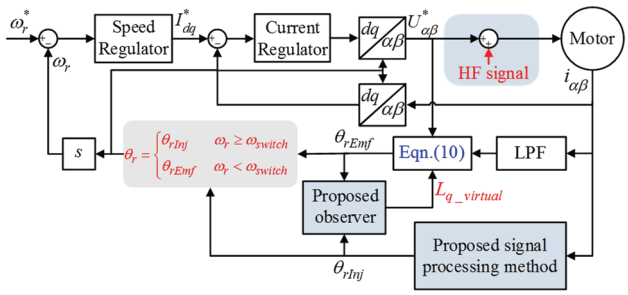

Fig. 6. Overall block diagram of the proposed sensorless control system.

The proposed control scheme can achieve sensorless MTPA control of IPMSMs in one step by defining and constructing a proper virtual q-axis inductance to directly calculate the current space vector angle along the MTPA trajectory rather than the rotor position, which greatly simplifies the whole implementation process. In addition, the combination of these two parts can guarantee more stable and accurate sensorless MTPA operation and reduce the position estimation errors induced by machine parameter uncertainties since the resulting error only take effects once in a control cycle rather than twice in a traditional scheme.

The calculation of the virtual q-axis inductance in the transition process and in the MTPA control are presented in Table I.

V. EXPERIMENTAL RESULTS

In this section, the validity and practicality of the proposed sensorless transition control strategy based on a new observer are tested by experiments. A total block diagram of the implemented drive system is described in Fig. 6. The system setup for experimental testing is shown in Fig. 7. The specifications and parameters of the tested IPMSM are listed in Table II. Another electrical machine is used to provide the load torque. An incremental encoder with a resolution of 2500 line is equipped to provide the actual rotor position. The proposed seamless transition control strategy is implemented with a microprocessor ADSP-CM408. A three-phase IGBT inverter, supplied at a dc-link voltage of 310 V, feeds the IPMSM. The PWM switching frequency is 10 *kHz* and the dead time is set to 2.5μs. The current sampling frequency is the same as the PWM switching frequency 10 *kHz*. The amplitude V_c and frequency ω_c of the high frequency

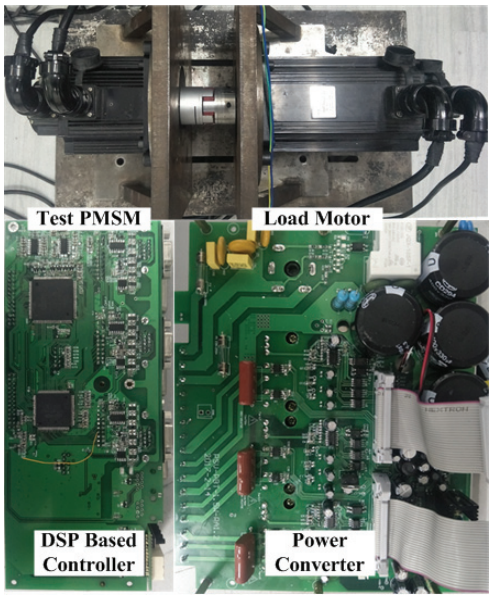

Fig. 7. Experimental setup used to test the proposed methods.

TABLE II
MOTOR PARAMETERS

Parameter	PMSM
Rated Power	2.2*kW*
Rated Speed	1500*r/min*
Rated Current	8.0*A*
Phase Resistance	0.418Ω
d-/*q*-axis Inductance	6.5*mH*/9.5*mH*
Pole Numbers	8
Rated Voltage	220*V*

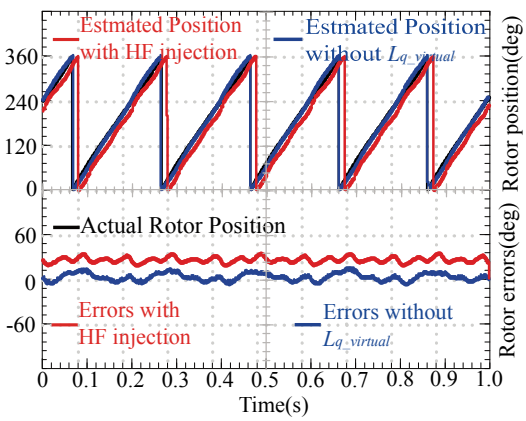

Fig. 8. Experimental results based on the high frequency carrier signal injection method and the fundamental model of the PMSM without $L_{q\_virtual}$ at the same rotor position.

injection voltage are selected as 50*V* and 500*Hz*, respectively. The switch speed ω_{switch} is calculated as 5*Hz*, which is equivalent to 75*r/min* when the pole numbers of the test motor are 8. All of the experimental results are obtained by an oscilloscope by using D/A modules.

Firstly, Fig. 8 shows experimental results based on the high frequency carrier signal injection method and a fundamental

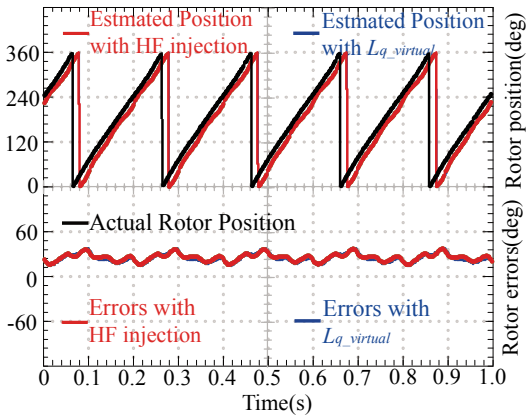

Fig. 9. Experimental results based on the high frequency carrier signal injection method and the fundamental model of the PMSM with $L_{q\_virtual}$ at the same rotor position.

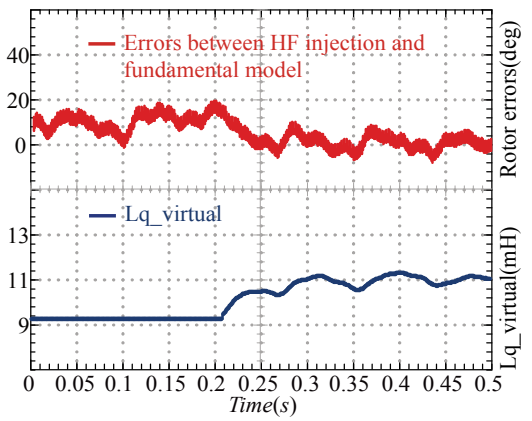

Fig. 10. Experimental results of a TP-PLL and the convergence procedure of $L_{q\_virtual}$.

model of the PMSM without the virtual *q*-axis inductance $L_{q\_virtual}$. The machine runs at 75*r/min*. It can be observed from the obtained experimental results that there are angle errors of about 20 degrees among the estimated rotor position θ_{rEmf} based on the fundamental model of the PMSM without the virtual *q*-axis inductance $L_{q\_virtual}$, the estimated rotor position θ_{rInj} based on the high frequency position θ_{rEmf} based on the fundamental model of the PMSM without the virtual *q*-axis inductance $L_{q\_virtual}$, and the estimated rotor position θ_{rInj} based on the high frequency carrier signal injection method. Meanwhile, θ_{rEmf} can track θ_{rInj} well when $L_{q\_virtual}$ is applied in the method based on the fundamental model of the PMSM, as shown in Fig. 9.

Fig. 10 shows the zoomed transition process between Fig. 8 and Fig. 9. It is obvious that the TP-PLL works well and that $L_{q\_virtual}$ soon changes to a stable value. At the same time, the estimated position error between the HF injection method and the fundamental model method tend to be zero. It only takes 80ms for the TP-PLL to track the angle.

In order to show comparisons between direct transition, a weighting function based transition scheme and the proposed transition strategy for sensorless applications. Experiments

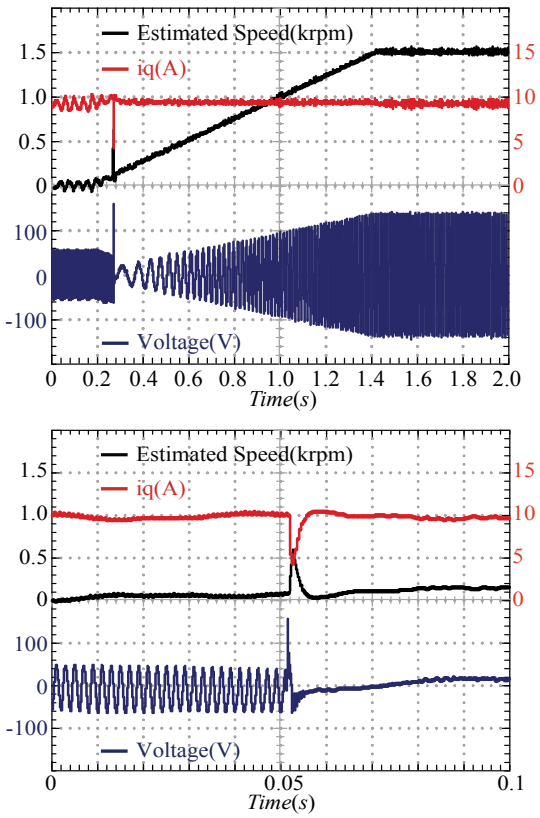

Fig. 11. Experimental results of a direct transition from θ_{rInj} to θ_{rEmf} with zoomed in transition process details.

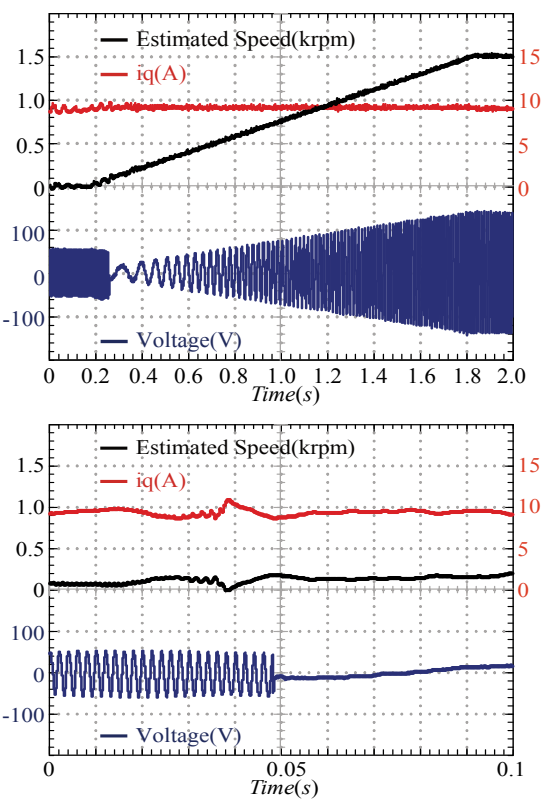

Fig. 12. Experimental results of a transition based on a weighting function to blend θ_{rInj} and θ_{rEmf} with zoomed in transition process details.

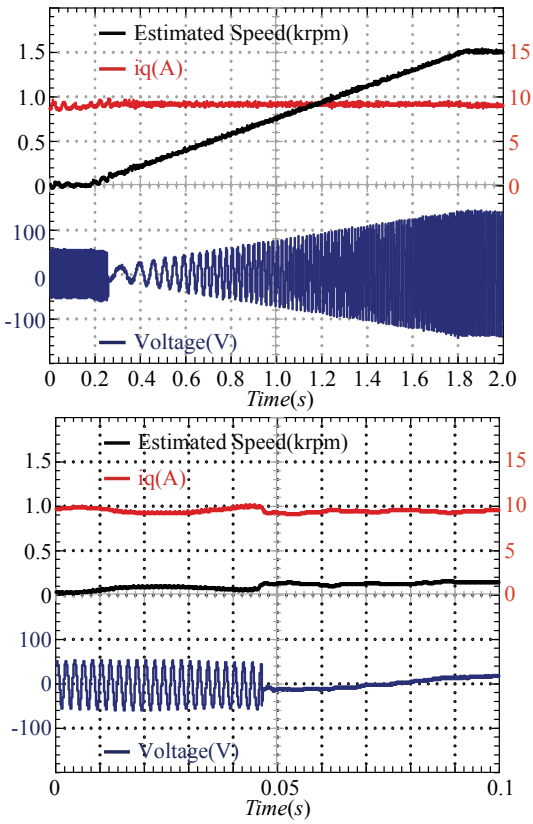

Fig. 13. Experimental results of the proposed transition strategy based on a TP-PLL.

are conducted with a rated load from startup to a rated speed of (1500*r/min*) in 2s in Fig. 11-13. Both the bandwidth of the observers using HF injection and the observers based on fundamental models in these 3 experiments are set the same to ensure a fair comparison. Thus, the differences only point to the transition section.

Fig. 11 shows both the speed and current vibrate just after the direct switch from the high frequency carrier signal injection method to the fundamental model based method. They are caused by sudden changes of rotor and speed from the 2 methods discussed in Section II.D.

Fig. 12 and Fig. 13 both show fairly smooth transitions without any obvious oscillations when compared with Fig. 11. The transition region is selected as 5Hz~6Hz, where the accuracy of the 2 sensorless methods can be guaranteed in Fig. 12. When it comes to the zoomed in parts, it is possible to find a little overshoot current during the transition region for Fig. 12. Meanwhile, the proposed method shows very fast transients and almost no fluctuations in Fig. 13. This verifies the effectiveness and good performance of the proposed sensorless transition control strategy.

VI. Conclusions

Hybrid rotor position estimation methods integrating a fundamental machine model and high frequency (HF) signal injection are widely used for interior permanent-magnet

synchronous machines (IPMSMs) for sensorless control in the entire speed range. However, the direct transition of two different methods may lead to system fluctuations or system instability since two estimated rotor positions based on two different rotor position methods are always unequal due to the effects of the parameter variations, system delays and inverter nonlinearities. In order to avoid these problems, a seamless transition strategy to define and construct a virtual q-axis inductance is proposed in this paper. With the proposed seamless transition strategy, the estimated rotor position based on the fundamental model is forced to track that based on HF signal injection before switching by adjusting the constructed virtual q-axis inductance. Meanwhile, since the virtual q-axis inductance changes with the rotor position estimation errors, a new observer with a TP-PLL is developed to accurately obtain the virtual q-axis inductance online. Furthermore, the sensorless control of IPMSMs with MTPA operations can be tracked automatically by selecting a proper virtual q-axis inductance. Finally, the feasibility and effectiveness of the proposed seamless transition strategy are validated on an IPMSM.

ACKNOWLEDGMENT

The authors gratefully acknowledge the support of the Foundation of State Key Laboratory of Coal Combustion (FSKLCCA1810).

REFERENCES

[1] J. M. Guerrero, M. Leetmaa, F. Briz, A. Zamarron, and R. D. Lorenz, "Inverter nonlinearity effects in high-frequency signal-injection-based sensorless control methods," *IEEE Trans. Ind. Appl.*, Vol. 41, No. 2, pp. 618-626, Mar./Apr. 2005.

[2] D. D. Reigosa, P. Garcia, D. Raca, F. Briz, R.D. Lorenz, "Carrier-signal selection for sensorless control of pm synchronous machines at zero and very low speeds," *IEEE Trans. Ind. Appl.*, Vol. 46, No. 1, pp. 167-178, Jan./Feb. 2010.

[3] N. C. Park and S. H. Kim, "Simple sensorless algorithm for interior permanent magnet synchronous motors based on high-frequency voltage injection method," *IET Electric Power Appl.*, Vol. 8, No. 2, pp. 68-75, Feb. 2014.

[4] S. C. Agarlita, I. Boldea, and F. Blaabjerg, "High frequency injection assisted "active-flux" based sensorless vector control of reluctance synchronous motors, with experiments from zero speed," *IEEE Trans. Ind. Appl.*, Vol. 48, No. 6, pp. 1931-1939, Nov./Dec. 2012.

[5] J. M. Liu and Z. Q. Zhu, "Novel sensorless control strategy with injection of high-frequency pulsating carrier signal into stationary reference frame," *IEEE Trans. Ind. Appl.*, Vol.50, No.4, pp.2574-2583, Jul./Aug. 2014.

[6] L. Xu, E. Inoa, Y. Liu. and B. Guan, "A new high-frequency injection method for sensorless control of doubly fed induction machines," *IEEE Trans. Ind. Appl.*, Vol. 48, No. 5, pp. 1556-1564, Sep./Oct. 2012.

[7] Y. C. Kwon and S. K. Sul, "Reduction of injection voltage in signal injection sensorless drives using a capacitor-integrated inverter," *IEEE Trans. Power Electron.*, Vol. 32, No. 8, pp. 6261-6274, Aug. 2017.

[8] W. Zine, X. Ge, and Y. C. Liu, "Optimisation of HF signal injection parameters for EV applications based on sensorless IPMSM drives," *IET Electric Power Appl.*, Vol. 12, No. 3, pp. 347-356, Mar. 2018.

[9] P. L. Xu and Z. Q. Zhu, "Novel square-wave signal injection method using zero-sequence voltage for sensorless control of PMSM drives," *IEEE Trans. Ind. Electron.*, Vol. 63, No. 12, pp. 7444-7454, Dec. 2016.

[10] H. Zhang, W. Liu, Z. Chen, G. Luo, J. Liu, and D. Zhao, "Asymmetric space vector modulation for PMSM sensorless drives based on square-wave voltage-injection method," *IEEE Trans. Ind. Appl.*, Vol. 54, No. 2, pp. 1425-1436, Mar./Apr. 2018.

[11] Y. Zhao, Z. Zhang, W. Qiao, and L. Wu, "An extended flux model-based rotor position estimator for sensorless control of salient-pole permanent-magnet synchronous machines," *IEEE Trans. Power Electron.*, Vol. 30, No. 8, pp. 4412-4422, Aug. 2015.

[12] K. B. Lee and F. Blaabjerg, "Improved sensorless vector control for induction motor drives fed by a matrix converter using nonlinear modeling and disturbance observer," *IEEE Trans. Energy Convers.*, Vol. 21, No. 1, pp. 52-59, Mar. 2006.

[13] Y. Park and S. K. Sul, "Sensorless control method for PMSM based on frequency-adaptive disturbance observer," *IEEE J. Emerg. Sel. Topics Power Electron.*, Vol. 2, No. 2, pp. 143-151, Jun. 2014.

[14] M. Habibullah and D. D. C. Lu, "A speed-sensorless FS-PTC of induction motors using extended kalman filters," *IEEE Trans. Ind. Electron.*, Vol. 62, No. 11, pp. 6765-6778, Nov. 2015.

[15] N. K. Quang, N. T. Hieu, and Q. P. Ha, "FPGA-based sensorless PMSM speed control using reduced-order extended Kalman filters," *IEEE Trans. Ind. Electron.*, Vol. 61, No. 12, pp. 6574-6582, Dec. 2014.

[16] E. Zerdali and M. Barut, "The comparisons of optimized extended Kalman filters for speed-sensorless control of induction motors," *IEEE Trans. Ind. Electron.*, Vol. 64, No. 6, pp. 4340-4351, Jun. 2017.

[17] R. Kumar, S. Das, P. Syam, and A. K. Chattopadhyay, "Review on model reference adaptive system for sensorless vector control of induction motor drives," *IET Electric Power Appl.*, Vol. 9, No. 7, pp. 496-511, Aug. 2015.

[18] C. Lascu, I. Boldea, and F. Blaabjerg, "A class of speed-sensorless sliding-mode observers for high-performance induction motor drives," *IEEE Trans. Ind. Electron.*, Vol. 56, No. 9, pp. 3394-3403, Sep. 2009.

[19] T. Bernardes, V. Foletto Montagner, H. A. Grundling, and H. Pinheiro, "Discrete-time sliding mode observer for sensorless vector control of permanent magnet synchronous machine," *IEEE Trans. Ind. Electron.*, Vol. 61, No. 4, pp. 1679-1691, Apr. 2014.

[20] C. Silva, G. M. Asher, and M. Sumner, "Hybrid rotor position observer for wide speed-range sensorless PM motor drives including zero speed," *IEEE Trans. Ind. Electron.*, Vol. 53, No. 2, pp. 373-378, Apr. 2006.

[21] G. D. Andreescu, C. I. Pitic, F. Blaabjerg, and I. Boldea,

"Combined flux observer with signal injection enhancement for wide speed range sensorless direct torque control of IPMSM drives," *IEEE Trans. Energy Convers*., Vol. 23, No. 2, pp. 393-402, Jun. 2008.

[22] M. Seilmeier and B. Piepenbreier, "Sensorless control of PMSM for the whole speed range using two-degree-of-freedom current control and hf test current injection for low-speed range," *IEEE Trans. Power Electron*., Vol. 30, No. 8, pp. 4394-4403, Aug. 2015.

[23] B. Du, S. Wu, S. Han, and S. Cui, "Application of linear active disturbance rejection controller for sensorless control of internal permanent-magnet synchronous motor," *IEEE Trans. Ind. Electron*., Vol. 63, No. 5, pp. 3019-3027, May 2016.

[24] S. C. Yang and Y. L. Hsu, "Full speed region sensorless drive of permanent-magnet machine combining saliency-based and back-EMF-based drive," *IEEE Trans. Ind. Electron*., Vol. 64, No. 2, pp. 1092-1101, Feb. 2017.

[25] Y. Sun, M. Preindl, S. Sirouspour, and A. Emadi, "Unified wide-speed sensorless scheme using nonlinear optimization for IPMSM drives," *IEEE Trans. Power Electron.*, Vol. 32, No. 8, pp. 6308-6322, Aug. 2017.

[26] Q. Tang, A. Shen and P. Luo, H. Shen, W. Li, and X. He, "IPMSMs sensorless MTPA control based on virtual Q-axis inductance by using virtual high frequency signal injection," *IEEE Trans. Ind. Electron.*, to be published. DOI: 10.1109/TIE.2018.2890487

Hanlin Shen was born in Jiangsu Province, China, in 1990. He received his B.S. degree from the School of Electrical and Information Engineering, Wuhan Institute of Technology (WIT), Wuhan, China, in 2013. He is presently working towards his Ph.D. degree in the School of Automation, Huazhong University of Science and Technology (HUST), Wuhan, China. His current research interests include power electronics, high-performance PMSM drives and motion control.

Jinbang Xu was born in Hubei Province, China, in 1973. He received his Ph.D. degree in Control Science and Engineering from the Department of Control Science and Engineering, Huazhong University of Science and Technology (HUST), Wuhan, China, in 2004. He is presently working as a professor in the School of Automation, HUST. His current research interests include power electronics, intelligent control and bioinformatics processing.

Baiqiang Yu received his B.S. degree in Automation from the School of Automation, Huazhong University of Science and Technology (HUST), Wuhan, China, in 2016, where he is presently working towards his Ph.D. degree in Control Science and Engineering. His current research interests include power electronics and motion control.

Qipeng Tang was born in Jiangxi Province, China, in 1991. He received his B.S. and Ph.D. degrees from the School of Automation, Huazhong University of Science and Technology (HUST), Wuhan, China, in 2013 and 2018, respectively. In 2018, he became a Post-Doctoral Researcher the College of Electrical Engineering, Zhejiang University, Hangzhou, China. His current research interests include power electronics, high performance ac motor drives and sensorless control for electrical drives.

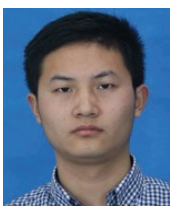

Bao Chen was born in Hubei Province, China, in 1993. He received his B.S. degree from the Huazhong University of Science and Technology (HUST), Wuhan, China, in 2015, where he is presently working towards his Ph.D. degree in the School of Artificial Intelligence and Automation. His current research interests include high performance ac motor drives and sensorless control for permanent-magnet synchronous machines.

Chun Lou is presently working as a Full Professor in the State Key Laboratory of Coal Combustion, School of Energy and Power Engineering, Huazhong University of Science and Technology (HUST), Wuhan, China. His current research interests include combustion measurement and instrumentation.

Yu Qiao is presently working as a Full Professor in the State Key Laboratory of Coal Combustion, School of Energy and Power Engineering, Huazhong University of Science and Technology (HUST), Wuhan, China. His current research interests include pollution control and energy utilization